EUROPEAN FUSION DEVELOPMENT AGREEMENT

EFDA–JET–PR(05)26

M.-L. Mayoral, P.U. Lamalle, D. Van Eester, E. A. Lerche, P. Beaumont,
E. De La Luna, P. De Vries, C. Gowers, R. Felton, J. Harling, V. Kiptily,
K. Lawson, M. Laxåback, P. Lomas, M.J. Mantsinen, F. Meo,
J.-M. Noterdaeme, I. Nunes, G. Piazza, M. Santala
and JET EFDA contributors

Hydrogen Plasmas with ICRF Inverted Minority Heating and Mode Conversion Regimes in the JET Tokamak

Hydrogen Plasmas with ICRF Inverted Minority Heating and Mode Conversion Regimes in the JET Tokamak

M.-L. Mayoral[1], P.U. Lamalle[2], D. Van Eester[2], E. A. Lerche[2], P. Beaumont[1], E. De La Luna[3], P. De Vries[1], C. Gowers[1], R. Felton[1], J. Harling[1], V. Kiptily[1], K. Lawson[1], M. Laxåback[4], P. Lomas[1], M.J. Mantsinen[5], F. Meo[6], J.-M. Noterdaeme[7, 8], I. Nunes[9], G. Piazza[10], M. Santala[5] and JET EFDA contributors[*]

[1]*Euratom/UKAEA Fusion Association, Culham Science Centre, Abingdon, Oxon, OX14 3DB, U.K.*
[2]*Association Euratom-Belgium State, LPP-ERM/KMS, B-1000 Brussels, Belgium*
[3]*Asociación Euratom-CIEMAT, Laboratorio Nacional de Fusion, Spain*
[4]*Euratom-VR Association, Sweden*
[5]*Helsinki U. of Technology, Tekes-Euratom Association, Finland*
[6]*Association Euratom-RISO, Riso National Laboratory, Denmark*
[7]*Max-Planck-Institut für Plasmaphysik, EURATOM-Assoziation, Germany*
[8]*EESA Lab, University Gent, Belgium*
[9]*Associação EURATOM/IST, Centro de Fusão Nuclear, Portugal*
[10]*Forschungszentrum Karlsruhe (FZK), Germany*
** See annex of J. Pamela et al, "Overview of JET Results ", (Proc.20 th IAEA Fusion Energy Conference, Vilamoura, Portugal (2004).*

Preprint of Paper submitted at
Nuclear Fusion Journal

ABSTRACT

During the initial operation of the International Thermonuclear Experimental Reactor (ITER), it is envisaged that activation will be minimised by using hydrogen (H) plasmas where the reference ion cyclotron resonance frequency (ICRF) heating scenarios rely on minority species such as helium (^{3}He) or deuterium (D). This paper firstly describes experiments dedicated to the study of 3He heating in H plasmas with a sequence of discharges in which 5MW of ICRF power was reliably coupled and the ^{3}He concentration, controlled in real-time, was varied from below 1% up to 10%. The minority heating regime was observed at low concentrations (up to 2%). Energetic tails in the ^{3}He distribution were observed with effective temperatures up to 300keV and bulk electron temperatures up to 6keV. At around 2%, a sudden transition was reproducibly observed to the mode conversion regime, in which the ICRF fast wave couples to short wavelength modes, leading to efficient direct electron heating and bulk electron temperatures up to 8keV. Secondly, the use of D minority ion heating in H plasmas was also investigated.This proved much more difficult since modest quantities of carbon C impurity ions, which have the same charge to mass ratio than the D ions, led directly to the mode conversion regime. Finally, numerical simulations with the 2-D full-wave code CYRANO, were used to further interpret some of the results obtained in these two sets of experiments.

1. INTRODUCTION

It is envisaged that, in the initial phase of International Thermonuclear Experimental Reactor (ITER) [1] operation, H plasmas will be used to minimise the activation of the machine during the commissioning stages. The two relevant ICRF scenarios foreseen in H plasmas are based on the heating of ^{3}He minority ions, referred to (^{3}He)H, or D minority ions, referred to (D)H. A key feature of these so-called inverted scenarios is that the minority ion species have a smaller charge to mass ratio than the majority ion species, i.e. $Z_{min} / A_{min} < Z_{maj} / A_{maj}$. In the past, tritium (T) inverted scenarios in D plasmas with T and D fractions of 5% and 95% respectively, have been successfully tested during the 1997 JET DT campaign [2]. Further results were also obtained in the recent “Trace Tritium” campaign at JET [3], with tritium concentrations up to around 3.5%. Nevertheless, until now (^{3}He)H and (D)H scenarios were only scarcely documented [4].

ICRF heating commonly relies on the propagation of the fast magnetosonic wave (or fast wave (FW)) to transport energy from the plasma edge to the core. The FW dispersion relation in the cold plasma theory can be written as:

$$n_\perp^2 = \frac{[L - n_{//}^2][R - n_{//}^2]}{[S - n_{//}^2]},$$

where R, L and S quantities are the dielectric tensor components defined by Stix [5]; $n_\perp = k_\perp c/\omega$ is the refractive index perpendicular to the magnetic field where $k_\perp$ is the perpendicular wave number;

$n_{//} = k_{//}c/\omega$ is refractive index parallel to the magnetic field $k_{//}$ being the parallel wave number. The FW propagation is illustrated in Fig.1 for a two-species plasmas. Two heating scenarios are shown: an inverted one (^{3}He)H and a standard one (^{3}He)D. The FW cut-offs are found for $n_{//}^2 = R$ (cut-off associated with the right-hand polarised wave component) and $n_{//}^2 = L$ (cut-off associated with the left-hand polarised wave component). The cold FW resonance occurs for $n_{//}^2 = S$, which corresponds for a two species plasma to the ion-ion hybrid layer R_{ii} [6].

The mode conversion (MC) regime occurs if the incoming FW efficiently tunnels through the thin evanescence layer between the left cut-off and the ion-ion layer. Then, considering a finite temperature plasma, the FW can be mode converted to hot plasma waves near the ion-ion layer. The nature of these short wavelength waves depends on the plasma properties [7]. They can be kinetic Alfvén waves, ion Bernstein waves (IBW) or electromagnetic ion cyclotron waves (ICW), depending on the relative importance of temperature and poloidal field effects [8][9][10]. Their main common characteristic is that they are damped strongly on electrons by electron landau damping (ELD) because of the strong up- or down- shift of $n_{//}$ due to the presence of a finite poloidal magnetic field [11].

The minority heating (MH) regime occurs when the FW energy is dominantly absorbed at the ion cyclotron resonance layer R_{ic}. The minority ion cyclotron resonance condition can be written as $\omega - n\omega_{c_i} - k_{//}v_{//} = 0$, where ω is the ICRF wave frequency; ω_{c_i} is the minority ion cyclotron frequency; n is the harmonic number and $v_{//}$ is the minority ion parallel velocity. In this regime, the FW absorption by the minority ions results in the formation of a high-energy population, i.e. the appearance of a tail in the minority ions distribution function. The heating of the background ions and electrons takes place on the rather long time scale of the fast minority ions collisional slowing-down time (typically of the order of 0.4s for the ^{3}He ions in the experiments described in this paper). When the energy of the fast minority ions is above a certain critical energy E_{crit} [5], the electrons are predominantly heated by collisions with the fast ions, whereas in the opposite case mainly ion heating is obtained.

In standard scenarios with the $Z_{min} / A_{min} > Z_{maj} / A_{maj}$, the ion-ion layer is located on the high field side (HFS) of the minority ion cyclotron resonance layer. In this case, the FW launched from low field side (LFS) antennas encounters the minority ion cyclotron resonance layer first. MH is the main heating scenario unless the minority concentration exceeds a critical value above which the fast wave electric field component E_+, which rotates in the same direction as the minority ions, is significantly reduced at the minority layer. Consequently, as the single-pass minority damping decreases significantly, a larger fraction of the FW can be mode-converted at the ion-ion layer. In JET, optimal concentration for MC regime in D plasmas with ^{3}He ions was found in the range of 12-20% [12].

In inverted scenarios, the cold plasma theory places the ion-ion layer and the associated left cut-off between the minority ion cyclotron resonance and the LFS antenna [13] [14] (see illustration on Fig.1), with R_{ii} moving to the LFS as the minority ion concentration is increased. In this case it is not immediately obvious which will be the preferential heating regime. Above a certain minority

concentration, when the MH regime single-pass damping is very weak, the MC regime is expected to dominate. In particular, for high minority concentration (> 20%), and if the plasma configuration is chosen in such a way that the minority ion cyclotron resonance is not located in the plasma, it has been shown on various tokamaks that efficient MC heating could be obtained [15][16]. Nevertheless, at very low minority concentration, when R_{ic} and R_{ii} are near each other, it is not completely clear if the fast wave will be mode converted or absorbed by a minority ion population. Indeed, even if the ion-ion layer is the first encountered by the FW, MH regime can occur if the minority ions have temperature high enough to Doppler broaden the resonance out of the left cut-off.

In section 2, experiments in which the ^{3}He concentration was scanned from 0.5% to 10% in H plasmas will be described. The minority heating regime obtained for concentrations below 2% will be studied as well as the transition to the mode conversion regime. In section 3, experiments with D minority ions in H plasmas will be presented. The influence of carbon impurity ions in this scheme will be highlighted. Finally, in section 4, results from numerical simulations of these two heating schemes obtained with the 2-D full-wave code CYRANO will be shown.

2. ICRF HEATING OF H PLASMAS WITH 3HE MINORITY IONS

2.1. EXPERIMENTAL SET-UP.

The experiments were carried out in H plasmas (with a small concentration of D from wall recycling, estimated to be 1-2%) in the single-null divertor configuration at a magnetic field (Bt) of 3.6T, a plasma current (Ip) of 2MA and a central electron density (n_{e0}) around $3\ 10^{19}\ m^{-3}$.

As discussed in the introduction, the ^{3}He concentration is one of the critical parameters influencing the FW damping. Hence, its control and determination was crucial for these experiments. As ^{3}He gas is lost through transport, keeping the concentration at a specific level requires ^{3}He gas to be puffed into the machine during the discharge [12]. A very efficient way to do this is to use the JET real-time central controller (RTCC) in order to link a measurement of the ^{3}He density to the opening of the gas injection valve. This technique, developed in the last few years [17], has been successfully used in the experiments presented here to control the ^{3}He concentration down to levels as low as 1.8%. The ^{3}He concentration ($n_{^3He}/n_e$) was estimated from the effective charge of the ions and the relative concentration of the majority and minority ions measured using the respective characteristic light emission in the divertor. Iron, argon, nickel, oxygen and carbon impurities were taken into account through the radiation spectrometer data. It should be note that when a very low ^{3}He concentration (< 1%) was required it was only necessary to puff ^{3}He before the ICRF heating phase.

Up to 5MW of ICRF power (P_{ICRF}) was applied using the four JET A2 ICRF antennas [18] at a nominal frequency of 37MHz, positioning the fundamental ^{3}He cyclotron resonance layer $R_{ic}(^3He)$ near the plasma centre (see Fig.2). The four transmission lines of each of the four A2 antennas do not have exactly the same electrical length. Consequently, the four antennas are operated at slightly different frequencies around the nominal frequency (the operating frequencies are obtained by optimising the matching element lengths in vacuum, i.e. adjusting the trombone and stub lengths to

minimise the power reflected back to the generators). The exact frequencies used are summarised in Table 1 together with the corresponding ^{3}He cyclotron resonance major radii. In particular, because the frequency of antenna D differs significantly from the other three, a spread in the resonance position over a width of about 10cm is obtained. Dipole phasing (0 π 0 π) of the antennas was used to launch waves with a symmetric toroidal mode number (n_Φ) spectrum and with $|n_\Phi| \approx 27$ at the maximum of the antenna power spectrum. Asymmetric toroidal mode number spectra with $|n_\Phi| \approx 13$ at the maximum of the antenna power spectrum were obtained with +90° phasing (predominantly launched in the co-current direction) and −90° phasing (predominantly in the counter-current direction).

In all these shots 1.3MW of H neutral beam injection (NBI) was added in order to allow measurements of ion temperature profiles using the edge charge-exchange diagnostic (the charge exchange diagnostic viewing the plasma core was not available for the experiments described).

In order to experimentally deduce the electron power deposition profiles, the electron temperature response to a modulation of the ICRF power was analysed using Fast Fourier Transform (FFT) and Break-In-Slope (BIS) methods [17][19][20]. The FFT technique is used to study the response of a system to a periodic perturbation. The BIS method requires only a step change in the power level to estimate the absorption profiles. The ICRF power was modulated during a 0.5s period at the beginning and at the end of the ICRF power flat-top with a frequency of 20Hz and an amplitude of 50% (see example on Fig.3). The electron temperature T_e was measured using an electron cyclotron emission (ECE) heterodyne radiometer [21] with the number of channels recently increased to 96 in order to cover approximately the full plasma radius. The time resolution varies from 0.2ms to 1ms, the estimated radial resolution for each individual channel is around 2-5cm and the separation between channels lower than 1cm. Ever since the installation of the divertor, the centre of JET plasmas have been typically displaced vertically with respect to the equatorial plane of the tokamak. As a consequence, the ECE line of sight (located about 0.13m above the machine midplane) passes below the magnetic axis by about 0.17m (cf. Fig.2). When doing FFT and BIS analysis, two radial co-ordinates are available for data interpretation:

- The actual major radius position at which the measurement is made.
- The major radius position corresponding to the intersection of the magnetic surface on which the measurement is made with the horizontal plane passing through the magnetic axis.

The second of these co-ordinates will be used for the electron power deposition profiles presented in this paper as it illustrates the fact that the plasma core is not diagnosed, thus avoiding misinterpretation of the data. Moreover, as fast time evolution of the density profiles is not available, it was assumed that this quantity does not respond to the rapid changes of the modulated ICRF power. The total fraction of the ICRF power damped directly on electrons was estimated by integrating the measured electron power density profiles over the plasma volume. Both methods assume that transport processes occur on a time scale much longer that the modulation period [20][22].

Finally, information on the presence of fast ICRF-accelerated ions was obtained with gamma-ray (γ-ray) spectrometry analysis [23] and both low-energy and high-energy neutral particle analysis (NPA)[24].

2.2. ^{3}HE MINORITY HEATING REGIME IN H PLASMAS

To establish the feasibility of ^{3}He MH regime in inverted scenarios a set of discharges were obtained with ^{3}He concentration below 2%. Figure 3 shows an overview of three discharges with $n_{^3He}/n_e<1\%$ and different phasings of the ICRF waves: dipole, +90º and –90º. Clear signatures of an efficient ^{3}He MH regime were obtained. A maximum electron temperature T_e^{max} of 6.2keV was reached with +90º phasing and P_{ICRF} 5MW. Central ion temperature measurements were not available for these experiments. Nevertheless, as illustrated in Fig.4, X-ray crystal spectrometer data were collected at a major radius R = 3.25m giving an ion temperature, $T_i(3.25m) \approx 2keV$ to be compared with an electron temperature at the same location of $T_e(3.25m) \approx 3.4keV$. Assuming standard L-mode profiles, one can then conclude that mainly electron heating was obtained with $T_i < T_e$.

The presence of a fast ^{3}He ion population led to an increase of the neutron rate (R_{NT}) which, in H plasmas, comes from the nuclear reaction between the beryllium impurities and ^{3}He ions, i.e. $^9Be(^3He,n)^{11}C$. A much higher neutron rate was obtained for the Pulse No: 63313 (+90º phasing) indicating a higher energy ^{3}He population compared to Pulses 63312 (dipole phasing) and 63314 (–90º phasing), which have similar ICRF power, ^{3}He concentration and electron density. The fast ^{3}He ion energy content (W_{fast}) defined as the perpendicular energy content in excess of two times the parallel value, i.e. $W_{fast} = W_\perp - 2W_{//}$, was estimated as four third of the difference between the total plasma energy derived from diamagnetic loop measurements $W_{DIA} = 3/2W_\perp$, and the total plasma energy derived from magnetic calculations, $W_{MHD} = 3/4W_\perp + 3/2W_{//}$, i.e. $W_{fast} = 4/3 (W_{DIA} - W_{MHD})$. This calculation gave a fast ^{3}He ion energy content up to 60% higher in the +90º case than in the –90º and dipole cases.

More information on the fast ^{3}He ion population was obtained from the γ-rays produced by the nuclear reactions, firstly between ^{3}He ions with energy above 0.9MeV and ^{9}Be impurity ions and secondly between ^{3}He ions with energy above 1.3MeV and 12C impurity ions [23]. The presence of a higher energy ^{3}He tail with +90º phasing was confirmed by the higher γ-ray emissivity (shown on Fig.5) for Pulse No: 63313 than for pulses 63312 (dipole phasing) and 63314 (–90º phasing). In Pulse No: 63319, also shown on Fig.5, the ^{3}He concentration was doubled with respect to shot 63313. The increase by a factor of 1.7 in the γ-ray signal and neutron rate confirmed a higher fast ion population but with a lower temperature tail. In this shot it was estimated that the tail temperature was $T_{tail} \approx 0.3 \pm 0.1MeV$.

The presence of ICRF accelerated ^{3}He ions was also illustrated by the R_{NT}, W_{DIA} and decrease (see Fig. 3 and Fig.5) following the decrease of the averaged ICRF power during the ICRF power modulation between t = 9s and t = 9.4s. High energy NPA data were collected that confirm a fast ^{3}He population but the fluxes of ^{3}He ions were too small to make any definite conclusions on the ^{3}He distribution function.

Information on the radial profile of the fast ^{3}He population was obtained from γ-ray emission profiles measured with the JET neutron and γ-ray diganostics [23], [25]. These consist of two cameras, vertical and horizontal, with nine and ten lines of sight, respectively. The line-integral measurements of the γ-ray emission along the lines of sight were tomographically reconstructed

[26] in order to give the local γ-ray emissivity in a poloidal cross section, as shown in Fig.6. The results obtained were found to be in agreement with the past observations of the ICRF-induced pinch effect expected when toroidally directed waves are used [27] [28][29]. In the +90º phasing case, the inward pinch of the resonating ions turning points produces, due to the detrapping of the resonant ion orbits, a significant number of high-energy non-standard passing ions on the low field side of the resonance [30]. In the –90º case, which corresponds to an ICRF-induced outward pinch, the standard trapped orbits dominate and the turning points of the orbits moves outwards along the resonance layer leading to a narrower and more elongated γ-ray profile (see Fig.6).

It should be noted that in both shots with +90º phasing (63313 and 63319), toroidal Alfvén eigenmodes (AEs) with frequencies between 220 and 260MHz were observed during the ICRF power flat-top while in the shots with dipole (63312) and –90º phasing (63314) no such activity was seen. Energetic ions can destabilise AEs with the drive proportional to the radial pressure gradient of the fast ions at the location of the mode when $n\omega_{fast} > \omega$. Here n is the toroidal mode number; ω is the mode frequency and ω_{fast} is the fast ion diamagnetic frequency, which is proportional to the radial pressure gradient of the energetic ions distribution function and increases with the effective tail temperature [31]. This suggests that the +90º phasing cases generated fast ions with more peaked radial pressure profiles and tails with energies high enough to excite AEs.

2.3. TRANSITION FROM ICRF MINORITY HEATING TO MC HEATING

As the ^{3}He concentration was increased above 2% a reproducible transition from the MH to the MC regime was observed. This transition to a different heating regime was seen on several diagnostic signals. First, as $n_{^3He}/n_e$ was increased, the T_e response to the ICRF power modulation gradually changed, indicating a change in the power deposition characteristics. In Fig.7, the time evolution of at R = 2.8m and the ^{3}He concentration are plotted for Pulse No: 63322 for which the ICRF modulation was applied throughout the ICRF power flat-top. One can clearly see a dramatic change in the response as became larger than 2% (t ≈ 8.2s). As discussed in the introduction, the finite slowing-down time of fast ions on the electrons in the MH regime leads to a delay in the temperature response with respect to the ICRF power modulation. In the MC regime, the electron heating is a direct process by ELD. Indeed, one can see in Fig.7(b) that, for $n_{^3He}/n_e \approx 3.2\%$, the T_e response was in phase with the power modulation, consistent with dominant direct electron heating. For $n_{^3He}/n_e \approx 0.8\%$ case (see Fig.7(a)), the period of the modulation of 0.05s associated with an estimated fast ^{3}He slowing down time of about 0.4s prevented us, as expected, from seeing any significant response.

The decrease in T_e observed after the transition between the two heating schemes (from t ≈ 8.5s) indicates that the optimal conditions for efficient electron heating are different in the MC and MH regimes. In the following section we will show results in which the experimental conditions have been optimised for the MC regime.

The transition between MH and MC was further confirmed by the disappearance of the fast ^{3}He population for $n_{^3He}/n_e > 2\%$. This was seen on the γ-ray emission (requiring ^{3}He ions with energy above 0.9MeV) shown in Fig.8 for the Pulse Nos: 63319, 63320 and 63324, which differ only in

^{3}He concentration. In discharge 63319, a high signal was measured throughout the pulse as the ^{3}He concentration stayed below 1.8%. In Pulse No: 63320, as $n_{^3He}/n_e$ increased above 2% for $t \approx 6.3$s the γ-ray signal began to decrease to finally disappear. Almost no signal was collected in Pulse No: 63324. One can also notice in Fig.8, the small decrease in ICRF power for Pulse No: 63320 and the very ragged ICRF power for Pulse No: 63324. This perturbation in the power was due to strong modification in the coupling resistance (representing the resistive part of the antenna loading) as the ICRF wave absorption mechanism changed at the transition bewteen the two regimes.

The critical 2% limit was also confirmed by plotting the fast ions energy content for a large range of pulses with different ICRF phasing, total heating power and magnetic field as a function of the ^{3}He concentration (see Fig.9). It should be noted that there were insufficient data available to document more precisely the heating regime transition between $n_{^3He}/n_e = 2\%$ and $n_{^3He}/n_e = 2.5\%$ or observe an effect of the wave phasing on the concentration level at the transition . Indeed, the transition between the two regimes is related to the Doppler broadening of the resonance. As this broadening is a function of $k_{//}$, one could expect a small difference in the ^{3}He concentration transition values with different antenna phasings.

An estimate of the electron deposition profiles before and after the change of heating regime was obtained with a BIS analysis of the Pulse No: 63322 (previously presented in Fig.7) and for which the ICRF power modulation was applied throughout the ICRF flat-top. As mentioned in the introduction, the BIS profiles were mapped onto the equatorial plane of the plasma. This is illustrated on the poloidal cross-sections presented in Fig.13, where one can see that no temperature measurements were available for major radius between 2.9m and 3.1m. Two of the electron deposition radial profiles are shown in Fig.10, corresponding to the times before and after the heating regime transition. For $n_{^3He}/n_e \approx 0.8\%$, a broad profile was obtained which seems to peak towards the undiagnosed plasma centre. This is consistent with indirect electron heating from the fast ^{3}He ions created at the cyclotron resonance layer $R_{ic}(^3He) \approx 2.94$ - 3.06m. Nevertheless, the deposition profile obtained was too broad to be explained by this heating alone and the method used to deduce it has been investigated more carefully. Indeed, the deposition profiles represented in Fig.10 were obtained from an upgraded BIS method [32], in which the phase lags between the power modulation and the electron temperature response, that occur during indirect electron heating, are taken into account. This was not the case in past experiments for which the standard BIS method, which neglects the phase lag, was used. With the standard BIS method, inconsistencies between the FFT and BIS predictions could be used as a diagnostic to indicate where indirect heating was taking place [20]. In order to investigate the reason behind the very broad profile obtained at low ^{3}He concentration, the three methods were compared and the resulting electron deposition profiles are shown in Fig.11. Between R = 3.0m and R = 3.3m, the FFT analysis and the new BIS analysis agreed but were both in disagreement with the standard BIS analysis, indicating indirect electron heating. From R = 3.3m and on the LFS, the three methods agreed, indicating dominant off-axis direct electron heating, peaked around 3.3m. Another indication of direct electron heating near R = 3.3 – 3.4m is seen in Fig.12, where the time delays between the temperature response and

the power modulation, obtained from the new BIS method, are shown as a function of the major radius. A clear decrease in the time delay is found near R = 3.3 – 3.4m. The reason for such off-axis direct electron heating was found to be the presence of C impurity ions in the plasma, which have the same charge to mass ratio as the D minority ions. The C concentration (n_c/n_e) was estimated to be 2-3%. These two ion species have, together, the same effect on the fast wave propagation as a much higher D concentration. A new ion-ion hybrid layer appears in the plasma where the FW can by mode converted. In Fig.13(a) this new ion-ion hybrid layer is illustrated in the case 2% of C and 2% of D in a H plasma, with an additional 0.8% of ^{3}He. The other plasma parameters were similar to Pulse No: 63322. The resulting direct absorption on the electrons HFS at R ≈ 2.6m was then observed on the same flux surface LFS at R ≈ 3.3m. The integrated power dissipated on the electrons was estimated to be 22% from standard BIS method or 32% from the new BIS method. Simulations presented in section 4 of this paper will also confirm the presence of this ion-ion hybrid layer and its influence.

For a higher ^{3}He concentration, $n_{^3He}/n_e$ 2.6%, the power deposition profiles on electrons (Fig.10 and Fig.13(b)) were much more peaked and located at a major radius around 3.15m, in agreement with the location of the ion-ion hybrid layer associated with 2.6% of ^{3}He in a H plasma (and other plasmas parameters like Pulse No: 63322). The integrated power transferred to the electrons compared with the total ICRF power absorbed by the plasma was estimated to be 60%, 69% and 71% from the standard BIS, the FFT and the new BIS methods respectively.

2.4. MODE CONVERSION REGIME IN H PLASMAS

In order to further investigate the MC regime and to optimise the conditions for efficient electron heating, experiments were performed with a magnetic field lowered to 3.3T and a ^{3}He concentration of 3.5%. The resulting ion-ion layer was located at a major radius R ≈ 2.8m instead of R ≈ 3.15m, which was the case in the previously discussed pulses. NBI power and therefore T_i measurements were not available for these pulses.

An overview of the results obtained is presented in Fig.14 for dipole and +90° phasings. One can clearly see that almost no neutrons were produced, confirming that few, if any, ^{3}He ions were accelerated. The higher electron temperature, up to 8.5keV, was obtained in the dipole case. The electron power deposition profiles presented in Fig.15, show a much higher power density in the central part of the plasma for the dipole case, with up to 87% of the total power absorbed by the electrons.

Assuming that the mode converted waves were absorbed before $k_{//}$ has the time to change significantly, a first explanation for the higher temperature in the dipole case can be found by looking at the ratio between the wave phase velocity, $v_\Phi = \omega/k_{//}$, and the electron thermal velocity, $v_{the} = \sqrt{T_e/m_e}$. Indeed, when v_Φ is of the order of v_{the} strong localised electron damping of the wave is expected. By assuming a target temperature of 3keV, one finds that the dipole case (with $k_{//} \approx |n_\Phi|/R_{ant} = 6.6m^{-1}$ and $R_{ant} \approx 4m$) gives $v_\Phi / v_{the} \approx 0.8$ as compared with the less favourable +90° case ($k_{//} \approx 3.3m^{-1}$) for which $v_\Phi / v_{the} \approx 0.8$.

In order to further confirm this tendency, numerical simulations with the 1-D code TOMCAT [33] were performed. This code is based on a variational principle for studying one dimensional wave propagation and damping near the ion-ion hybrid conversion layer in tokamaks. Toroidal and oblique incidence effects are retained, but the poloidal magnetic field is neglected. Up to second order corrections in $k_\perp \rho_L$, where ρ_L is the Larmor radius, are kept. A double transit of the wave is assumed (i.e. the reflection of the transmitted power from the HFS cut-off is included). Simulations were performed for Bt = 3.3T, f_{ICRF} = 37MHz, $n_{e0} = 3\ 10^{19}\ m^{-3}$, for two ^{3}He concentration (2% and 3.5%) and three plasma target temperatures (3keV, 5keV and 8keV). The resulting total powers transferred to the electrons (Pe) and to the ^{3}He ions ($P_{^3He}$) are summarised in Table 2 and are consistent with the experimental behaviour. For $n_{^3He}/n_e = 3.5\%$, P_e is systematically higher for the dipole case than for the +90º case, with a maximum absorption for plasma target temperatures of 3 and 5keV. Interestingly, for the 8keV target, Pe is smaller. This result is consistent with the small decrease in Te observed experimentally from 6.2s to 6.75s for Pulse No: 63384 (cf.Fig.14).

3. ICRF HEATING OF D IONS IN H PLASMAS

The experimental set-up for these experiments was similar to the one described above. The experiments were carried out at a magnetic field of 3.9T, a plasma current of 2MA and a central electron density of $3\ 10^{19}\ m^{-3}$. The D minority concentration resulted from D ion desorption from the wall, the legacy of previous D plasma operation, and was estimated to be n_D/n_e = 1-2%. In order to position the fundamental D cyclotron resonance in the plasma centre (R ≈ 3.1m), ICRF waves at a nominal frequency of 29MHz were used. The exact operating frequencies for the four antennas and the corresponding fundamental D cyclotron resonances are summarised in Table 3. Dipole symmetric phasing was used.

An overview of a typical shot is presented in Fig.16. The coupling of the ICRF power was very challenging in this set of experiments and only brief peaks at a maximum value of 2.5MW were achieved. Most of the time the averaged coupled power was around 1.5MW. The first reason for this power limitation comes from the fact that 29MHz is near the limit of the generator capability. Furthermore, the coupling is very low in this frequency range (around 1Ohm) and the maximum voltage on the lines is easily reached, restricting the power that can be coupled.

Surprisingly, no D fast ions were detected, either by the neutral particle analyser or the γ-rays emission. No neutrons were detected and the maximum electron temperature obtained was around 3keV. BIS analysis performed on several shots revealed, as illustrated in Fig.17, a rather peaked electron power deposition profile with its maximum at R ≈ 3.5m and a full width at half maximum of around 30cm. The total power absorbed by the electrons was estimated to be around 50% of the ICRF power. This off-axis electron heating could only be explained by the presence in the plasma of 2-3% of C, leading directly to the mode conversion regime. The effect of 2% of C on the dispersion relation is shown on Fig.18. On Fig.18(a) the dispersion relation is plotted with n_D/n_e = 2% and in Fig.18(b) with n_D/n_e = 2% and n_C/n_e = 2%. The ion-ion hybrid layer is moved to the LFS by the addition of the carbon, being seen in Fig.18(b) at a major radius of around 3.5m. The fast wave is

then expected to be mode converted before reaching the D cyclotron resonance layer, preventing any D minority heating.

No optimisation of this mode conversion heating scheme was attempted because of the restrictions at the frequency used and the lack of control on the ion-ion hybrid layer position.

4. CYRANO SIMULATIONS

The modelling of these experiments is challenging due to the various types of waves that co-exist in the chosen experimental conditions. For the large scale fast wave, the finite Larmor radius approximation, $k_\perp \rho_L << 1$, is commonly used to simplify the plasma dielectric response in numerical simulations. Typically, in our experiments, $\rho_L \approx 0.3$cm for the ^{3}He ions and the perpendicular wavelength for the FW, $\lambda_\perp = 2\pi/k_\perp$, is around 35cm. However, for the small scale ion Berstein waves, for which one typically has $k_\perp \rho_L \approx 1$, the finite Larmor radius approximation, usually used to simplify the plasma dielectric response in numerical simulations, is not valid anymore. Finally, the ion cyclotron wave also exists and has yet a different behaviour.

CYRANO [34] is a 2-D full-wave code in toroidal geometry for the ICRF range of frequencies generally used in tokamaks. Maxwell's equations for the wave field (expanded in Fourier series in poloidal and toroidal directions) are solved on a radial mesh over the tokamak poloidal cross-section using a finite element method and account for the kinetic properties of the plasma dielectric response. Appropriate boundary conditions for the Fourier component of the fields are imposed at the machine wall and at the ICRF antenna. Corrections up to the second order in $\rho_L k_\perp$ are kept, which accounts for the fast, slow and Berstein wave dynamics. As poloidal field effects are accounted for, the ion cyclotron wave can be excited as well. While the propagation and the damping of the fast wave is expected to be correctly treated with a moderate number of radial points and poloidal Fourier harmonics, the correct treatment of the short wave branches is much more demanding. First, the poloidal resolution necessary to resolve such waves is far beyond our present computer capabilities without going to parallel processing. For example, if one considers a wavelength of 0.1cm, which can be easily reached for IBW, and assuming that one should have at least two points per wavelength to roughly represent the wave fields, one finds that, for a plasma with a minor radius of 1m, one would need around 1000 poloidal modes. Another drawback of the treatment arises due to the truncation of the finite Larmor radius effects in the plasma dielectric response. Such a procedure is only justified if $k_\perp \rho_L < 1$, which, as mentioned, is strictly only true for the fast waves.

4.1. H PLASMAS WITH ^{3}HE MINORITY IONS

For the (^{3}He)H experiments, the CYRANO simulations were performed with a magnetic field of 3.6T, a plasma current of 2MA, a central electron density of $3\ 10^{19}$ m^{-3} and an ICRF frequency of 37MHz. 50 poloidal modes were considered with toroidal mode number $n_\phi \approx -27$, corresponding to the maximum of the antenna power spectrum with a dipole phasing. In order to investigate the rather low ^{3}He concentration level obtained experimentally for the transition between the MH and the MC regime, simulations with a systematic increase in ^{3}He concentration were done ($n_{^3He}/n_e$ =

0.5%, 1%, 1.5%, 2%, 2.5%, 3%, 4%, 5%, 7% and 10%). Initially, for each ^{3}He concentration value, simulations with n_D/n_e = 0%, 1% and 2% were performed. No significant effect related to the presence of D was observed. Then, fixing the D concentration at 2%, the ^{3}He concentration scan was repeated with n_C/n_e = 1% and 2%. In this case, the results show that the percentage of C^{6+} present in the plasma can considerably influence the ICRF power absorption, in particular for very low ^{3}He concentration in the MH regime. The relative power fractions absorbed by the electrons and ^{3}He ions for 0% and 2% of C^{6+} (both with 2% of D) are presented in Fig.19.

Without carbon, the transition between the minority heating regime, for which the absorption on the ^{3}He is dominant, and the mode conversion regime occurs for $n_{^3He}/n_e \approx 5\%$. As soon as carbon impurity ions are included the ^{3}He level at which the transition occurs decreases. When 1% of carbon is assumed (not shown) the transition occurs at around $n_{^3He}/n_e$ 4%. With 2% of carbon the transition occurs near $n_{^3He}/n_e$ 3%, in reasonable agreement with the experimental value.

Another effect of the presence of carbon on the power partition between the ^{3}He ions and the electrons can be seen for low ^{3}He concentration (MH regime). In the absence of carbon (dashed line) and for $n_{^3He}/n_e < 3\%$, practically all the ICRF power is absorbed by the ^{3}He ions. However, when 2% of Carbon is added (solid lines), the simulations show that a significant fraction of the total power is already absorbed by the electrons, particularly for very low ^{3}He concentration ($n_{^3He}/n_e < 1.5\%$). As a matter of fact, this electron absorption, found in the simulations at low ^{3}He concentration, is in agreement with the experimental observation of direct electron heating in the MH regime associated with the mode conversion layer of D and C on the HFS. The resulting power fraction absorbed by the electrons is around 30% at $n_{^3He}/n_e$ = 0.5% and decreases with increasing ^{3}He concentration up to a minimum for $n_{^3He}/n_e$ = 1.5%, where the optimal conditions for MH regime are achieved. For higher ^{3}He concentrations the electron power fraction systematically increases and the absorption on the ^{3}He mode conversion layer becomes the major cause of direct absorption by electrons.

In order to illustrate further the influence of the carbon impurity ions at low ^{3}He concentration, the power deposition profiles (normalised to 1MW of total ICRF power), obtained for $n_{^3He}/n_e$ = 0.5%, 1%, 1.5% and 2%, are shown in Fig.20. For ^{3}He concentration of 0.5 % and 1 % (Fig.20(a) and Fig.20(b)), the electron absorption observed between ρ = 0.3 – 0.5 is in good agreement with the region of direct electron heating highlighted by the new BIS in, for example, Fig.12. For a ^{3}He concentration of 1.5% (Fig.20(c)) the minority ions absorption is very efficient and only a very small percentage of the power is directly absorbed by the electrons. At the beginning of the MC regime (Fig.20(d)) both ions and electrons share comparable amounts of the total ICRF power, the electrons now being heated near the MC layer associated with the ^{3}He ions. The location of the electron absorption is in good agreement with the maximum of the power absorption profiles obtained in paragraph 2.3 for Pulse No: 63322. Nevertheless, it is important to mention that the electron power deposition profiles obtained with CYRANO account for only non-collisional processes and that they cannot be straightforwardly compared with the experimental profiles showing both direct electron heating and indirect electron heating due to collisions with the fast ions.

Finally, it is clear that the simulations give underestimated values for the electron absorption for $n_{^3He}/n_e > 3\%$ compared with the experimental observation. This can be related to a rather poor description of the IBW due to the limited number of poloidal modes considered in the simulation, as already explained. Another important factor is that only one toroidal mode is considered while, in reality each component of the antenna spectrum contributes with different weight, to the overall power absorption observed experimentally.

4.2. H PLASMAS WITH D MINORITY IONS

The following CYRANO simulations were performed with a magnetic field of 3.9T, a plasma current of 2MA, a central electron density of 2.5 10^{19} m^{-3} and an ICRF frequency of 37MHz. 50 poloidal modes were used with toroidal mode numbers $n_\phi \approx 27$ and $n_\phi \approx -27$, corresponding to the peaks of the antenna power spectrum with a dipole phasing.

First, the D concentration was scanned between 0.5% and 7% without any carbon. It was found that, until around n_D/n_e = 3-4%, most of the power is indeed absorbed by the D minority ions near the D cyclotron resonance layer. For $n_D/n_e > 4\%$ the power directly absorbed by the electrons becomes dominant, corresponding to the transition to the MC regime. Figure 21, which shows the power density profiles obtained for the electrons and D ions, clearly illustrates the effect of adding 0.5% of carbon impurity ions to the 2% of D minority ions. The minority heating scenario, with dominant power deposition on the D minority ions, practically disappears. This emphasises the deleterious influence of even very small traces of carbon for the (D)H heating scheme. Again, the somewhat distorted deposition profiles in Fig.21(b) are probably connected to an inadequate number of poloidal modes to describe the IBW correctly.

CONCLUSIONS

Inverted minority scenarios relevant for the non-activated phase of ITER in H plasmas have been tested at JET. Due to the Doppler broadening of the ^{3}He cyclotron resonance, ^{3}He minority heating was successfully achieved for $n_{^3He}/n_e$ below 2%. When $n_{^3He}/n_e$ was increased further the mode conversion regime dominated. By positioning the conversion layer in the plasma centre, electron temperatures up to 8keV were obtained using dipole phasing. D minority heating in H plasmas was also tested. This scenario was not successful as the presence of carbon impurity ions led directly to far off-axis fast wave mode conversion. This effect, confirmed by the simulations with the full-wave code CYRANO, is expected to take place for carbon concentration as low as 0.5%, thus preventing an efficient absorption at the D minority cyclotron resonance layer. As the mode conversion layer position is very sensitive to small changes in the carbon concentration, ICRF heating relying on D minority may be found unusable for the non-active phase of ITER, probably making ^{3}He minority heating the best choice.

ACKNOWLEDGEMENT

This work has been conducted under the European Fusion Development Agreement. It is a pleasure

to thank our colleagues who operated the tokamak, the heating systems and the diagnostics during the experiments. The work carried out by the UKAEA personnel was jointly funded by the United Kingdom Engineering and Physical Sciences Research Council and by Euratom. The view and opinions expressed herein do not necessarily reflect those of the European commision.

REFERENCES

[1]. ITER Physics Basis Editors, ITER Physics Expert Group Chairs and Co-Chairs and ITER Joint Central Team and Physics Integration Unit, Nucl. Fusion **39**, (1999) 12

[2]. Start D.F.H. *et al*., Nucl. Fusion **39(3)** (1999) 321

[3]. Lamalle P.U. *et al.*, Proceedings of the 31st EPS Conference on Plasma Phys., London, 28 June - 2 July 2004, edited by P. Norreys and H. Hutchinson, European Physical Society, ECA Vol.**28G**, (2004) P-5.165

[4]. Lamalle P.U. *et al.*, accepted for publication in Nucl. Fusion (2005)

[5]. Stix T.H., Waves in plasmas (New York: American Institut of Physics)

[6]. Stix T.H, Plasma Phys. **14** (1972) 367

[7]. Perkins F.W., Nucl. Fusion **17(6)** (1977) 1197-1224

[8]. Nelson-Melby E. *et al.*, Phys. Rev. Lett. **90(15)** (2003) 155004

[9]. Jaeger E.F. *et al*, Phys. Rev. Lett. **90(19)** (2003) 195001

[10]. Lin Y. *et al.*, Plasma Phys. and Control. Fusion **45** (2003), 1013-1026]

[11]. Ram A.K. and Bers A., Phys. Fluids B **3** (1991) 10059-10069

[12]. Mantsinen M.J., Mayoral M-L., Van Eester D. *et al.*, Nucl. Fusion **44** (2004) 33-46

[13]. Stix T.H., Nucl. Fusion **15** (1975) 737

[14]. Majeski R., Phillips C.F., Wilson T.R., Phys. Rev. Lett **73** (1994) 2204.

[15]. Bonoli P. *et al.*, *Phys. Plasmas* **4(5)** (1997) 1774-1782

[16]. Saoutic B. *et al*., *Phys. Rev. Lett*. **76(10)** (1996)1647-1650

[17]. Van Eester D. *et al.*, Proceedings of 15th Conference on radio-Frequency Plasmas, Moran, Wyoming, 19-21 may 2003, edited by Cary B. Forest, American Institut of Physics, Melville, New–York, Vol. **694**, 2004.

[18]. Kaye A. *et al.*, Fusion Eng. Des. **24** (1994) 1

[19]. Gambier D.J. *et al*, Nucl. Fusion **30** (1990) 23-24

[20]. Van Eester D., Plasma Phys. and Control. Fusion **42** (2004) 1675-1697.

[21]. De la Luna E. *et al*,. Rev. Sci. Instrum. **75(10)** (2004) 3831-3833

[22]. Mantica P. *et al*., 2002, Fusion energy 2002 (Proceeding 19th Int. Conf., Lyon, 2002) EX/P1-04, IAEA, Vienna.

[23]. Kiptily V.G. et al, Nucl. Fusion **42** (2002) 999-1007

[24]. Korotkov A.A., Gondhalekar A. and Stuart A.J. 1997, Nuclear Fusion 37 35

[25]. Jarvis O. N. *et al*., Nucl, Fusion **36(11)** (1996), 1513-1530.

[26]. Ingesson L.C. *et al.*, Nucl. Fusion **38(11)** (1998) 1675-1694.

[27]. Chen L., Vaclavick J. and Hammett G., Nucl. Fusion **28(3)** (1988) 389-398
[28]. Eriksson L.-G. et al., Phys. Rev. Lett. **81(6)** (1998) 1231-1234
[29]. Mantsinen M.J. et al., Phys. Rev. Lett. **89(11)** (2002) 1150004-1
[30]. Hedin J., Hellsten T., Eriksson L.-G. and Johnson T., Nucl. Fusion **42** (2002) 527-540
[31]. Kener W. *et al.*, Nucl. Fusion **38(9)** (1998) 1315-1332
[32]. Lerche E. A., to be submitted to Plasma Phys. and Control. Fusion in 2005
[33]. Van Eester D. and Koch R., Plasma Phys. and Control. Fusion **40(11)** (1998) 1949-1976
[34]. Lamalle P.U., LPP-ERM/KMS Lab. Report **101**, Brussels (1994)

	Antenna A	**Antenna B**	**Antenna C**	**Antenna D**
Frequency (MHz)	37.2	37.3	37.4	36
$R_{ic}(^3He)$ (m) at 3.6T	2.94	2.96	2.97	3.06
$R_{ic}(^3He)$ (m) at 3.3T	2.64	2.68	2.69	2.78

Table 1: Operating frequencies for the four ICRF antennas and corresponding ^{3}He cyclotron resonance major radii, for B_t = 3.6T and 3.3T.

T_{en}(keV)	**[^{3}He] (%)**	**+90°**		**Dipole**	
		P_e (%)	**P_{3He} (%)**	**P_e (%)**	**P_{3He} (%)**
3	2	37.9	7.1	11.6	7.6
5	2	36.9	11.8	10.7	15.6
8	2	34.3	19.9	12.7	24.4
3	3.5	36.4	5.7	76.1	2.3
5	3.5	35.8	8	71.6	10.5
8	3.5	33.8	12.5	42.9	44.9

Table 2: Total electron and ^{3}He power heating power calculated using the TOMCAT simulation code for different plasma target temperature (3, 5 and 8keV) and ^{3}He concentration of 2 and 3.5%

	Antenna A	**Antenna B**	**Antenna C**	**Antenna D**
Frequency (MHz)	28.4	28.5	29.3	28.1
R_{ic}(D) (m) at 3.9T	3.11	3.1	3.02	3.14

Table 3: Operating frequencies for the four ICRF antennas and corresponding D cyclotron resonance major radii, for B_t = 3.9T.

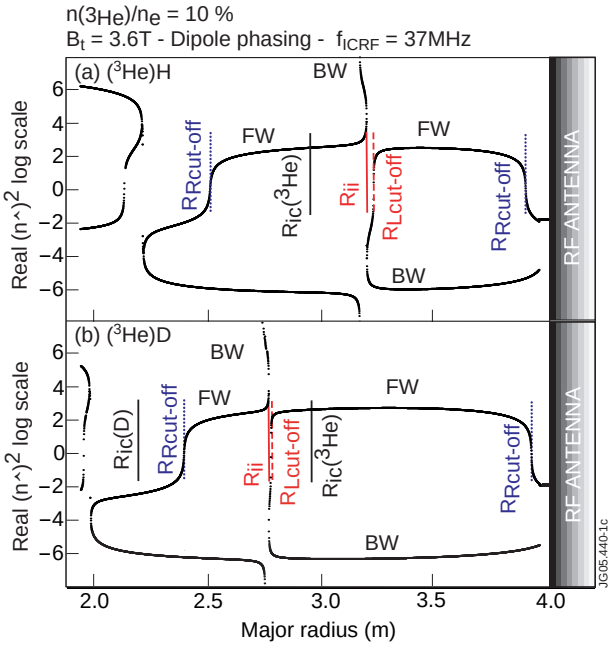

Figure 1: Real part of the perpendicular refractive index obtained from the resolution of the cold plasma dispersion relation. The following radial location are indicated: FW left cut-off $R_{Lcut\text{-}off}$; FW right cut-off $R_{Rcut\text{-}off}$; FW resonance R_{ii}; ion cyclotron resonance R_{ic} .(a) illustrates an inverted scenario (^{3}He)H and (b) a standard scenario (^{3}He)D.

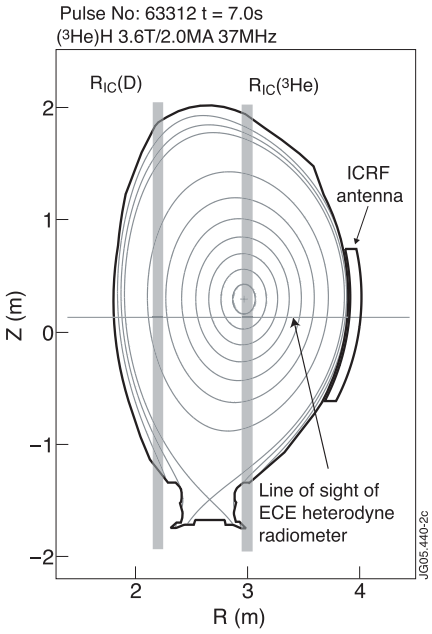

Figure 2: Tokamak poloidal cross-scetion with locations of the ^{3}He and D cyclotron resonance layers for Pulse No: 63312 with B_t = 3.6T and an ICRF frequency of 37MHz. The ICRF antenna and the line-of sight for the ECE electron temperature measurements are also shown.

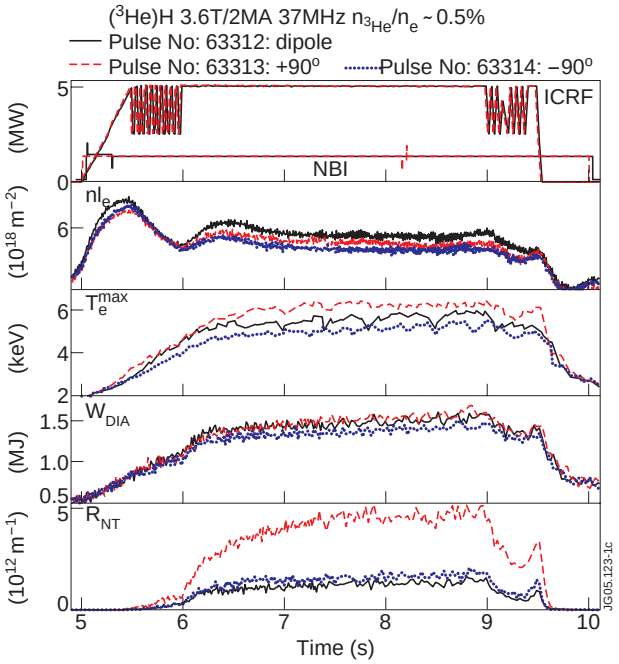

Figure 3: Time evolution of the ICRF and NBI power (H beams), central line integrated density from the far infrared interferometer diagnostic (the central density n_{e0}, from LIDAR Thomson Scattering, was for the Pulses 63312 and 63314 n_{e0} = 3 10^{19} m^{-3}; LIDAR data were not available for the Pulse No: 63313), maximum electron temperature from the ECE Michelson interferometer diagnostic, plasma diamagnetic stored energy and neutron rate from ^{9}Be(^{3}He,n)^{11}C reaction. Three discharges are represented for different ICRF wave phasing: dipole, +90° and –90°.

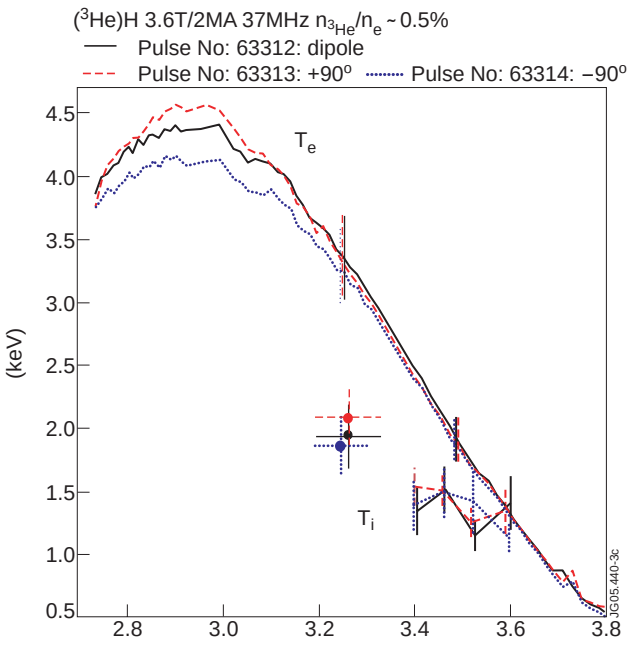

Figure 4: Radial profiles of the electron temperature (from the ECE heterodyne radiometer at around 0.17m below the magnetic axis). The ion temperature points at R = 3.25m is measured using a X-ray crystal spectrometer. The ion temperatures profiles at the plasma edge are measured using edge charge exchange recombination spectroscopy.

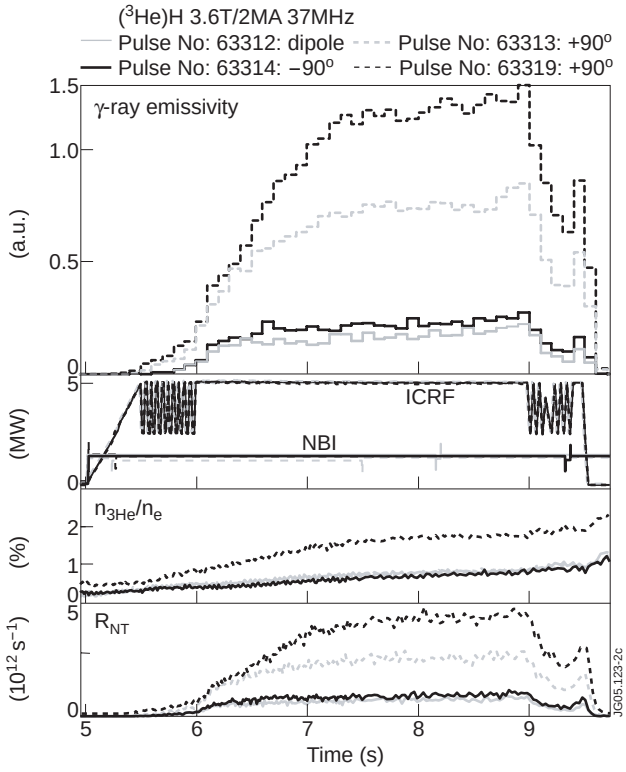

Figure 5: Time evolution of the γ-ray emissivity, ICRF and NBI power, ^{3}He concentration and neutron rate for pulses 63312 (dipole), 63313(+90°), 63314 (–90°) with ^{3}He concentration below 1% and Pulse No: 63319 (+90°) with ^{3}He concentration up to 1.8%.

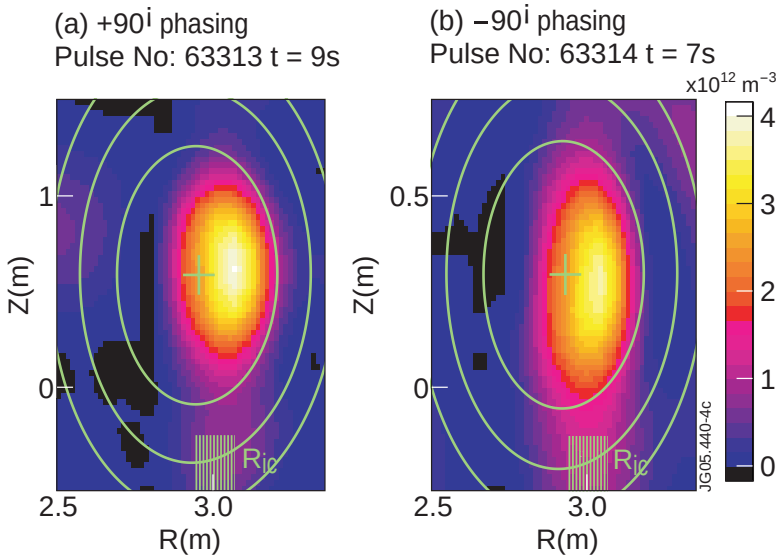

Figure 6: γ-ray emission profiles (normalised to the peak value) for a +90° phasing case (Pulse No: 63313) and a –90° phasing case (Pulse No: 63314). A number of flux surfaces are shown in green; a green cross indicates the magnetic axis. The ^{3}He ion cyclotron resonance is also represented.

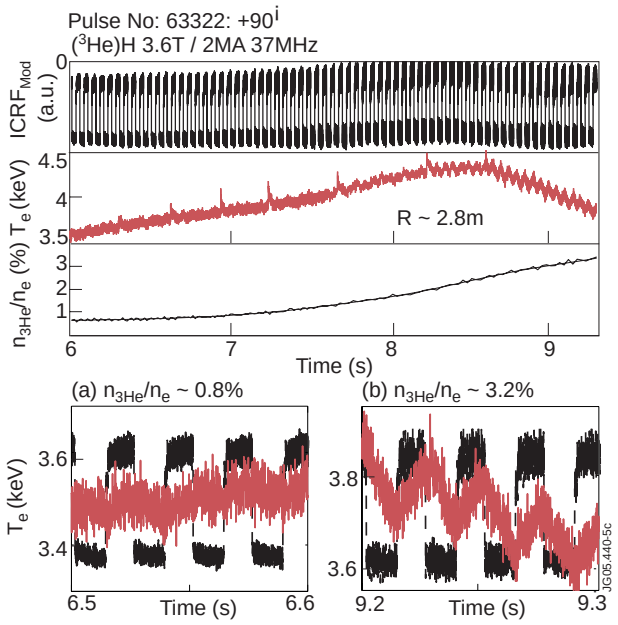

Figure 7: Time evolution of the ICRFpower modulation, electron temperature at R = 2.8m form ECE measurements and ^{3}He concentration for the Pulse No: 63322 (+90° phasing). Zooms on the electron temperature response to the ICRF power modulation are also represented for (a) $n_{3He}/n_e \approx 0.8\%$ and (b) $n_{3He}/n_e \approx 3.2\%$.

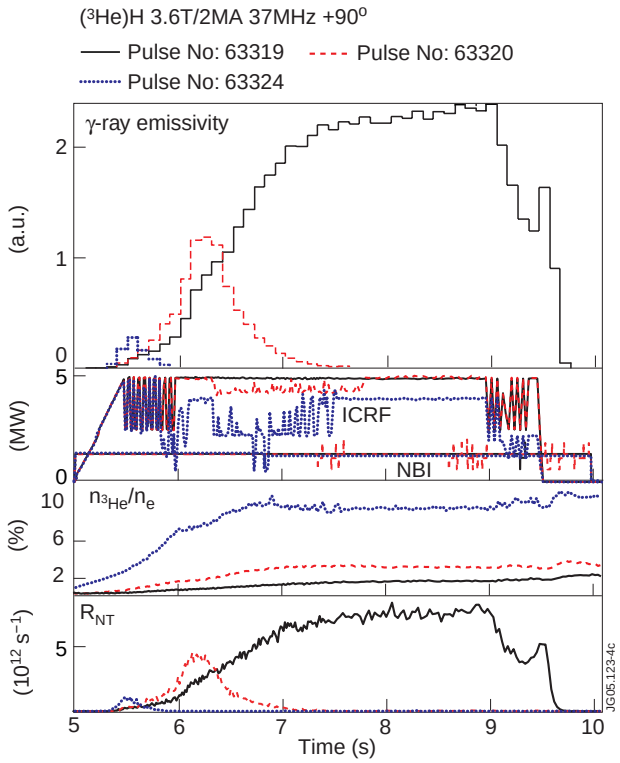

Figure 8: Time evolution of the γ-ray emissivity, ICRF and NBI power, ^{3}He concentration and neutron rate for pulses 63319, 63320, 63324.

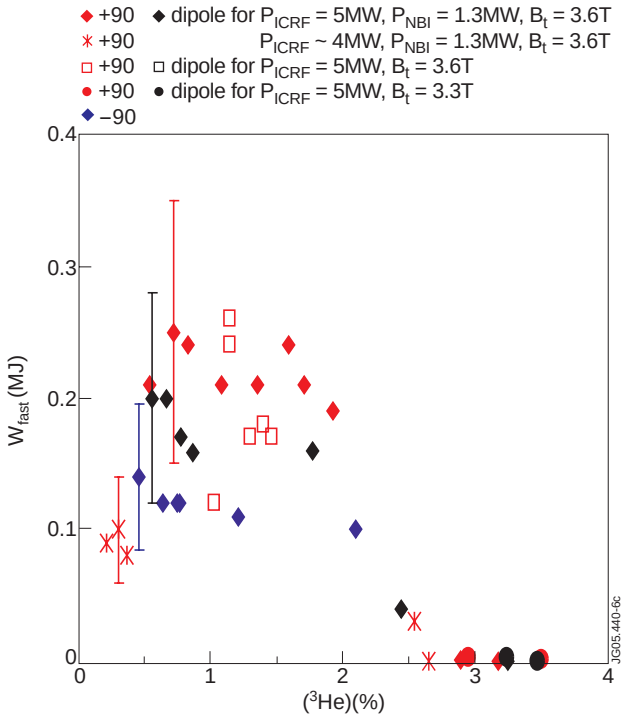

Figure 9: Fast ions energy content as a function of the ^{3}He concentration for a set of shots with different ICRF phasings, total heating power and toroidal magnetic field. $W_{fast} = W_\perp - 2W_{//}$ was derived from the total plasma energy from diamagnetic measurements, $W_{DIA} = 3/2\, W_\perp$, and from magnetic calculations, $W_{MHD} = 3/2\, W_\perp + 3/2\, W_{//}$, i.e. $W_{fast} = 4/3\, (W_{DIA} - W_{MHD})$.

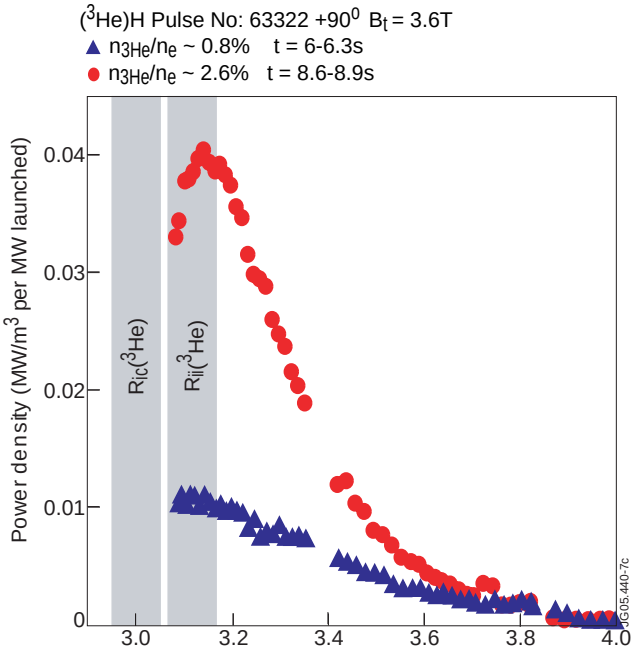

Figure 10: Electron deposition profiles from BIS analysis at two different ^{3}He concentrations for the Pulse No: 63322. The triangles correspond to $n_{3He}/n_e \approx 0.8\%$ (MH regime). The dots correspond to $n_{3He}/n_e \approx 2.6\%$ (MC regime).

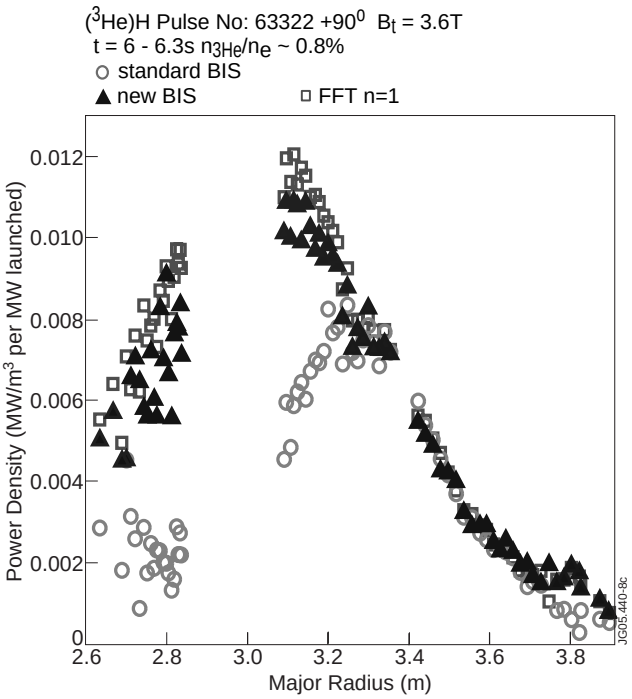

Figure 11: Electron deposition profiles from three different methods. The new BIS analysis takes into account delays in the electron temperature response to the ICRF power modulation. Good agreement between the three methods indicates direct electron heating.

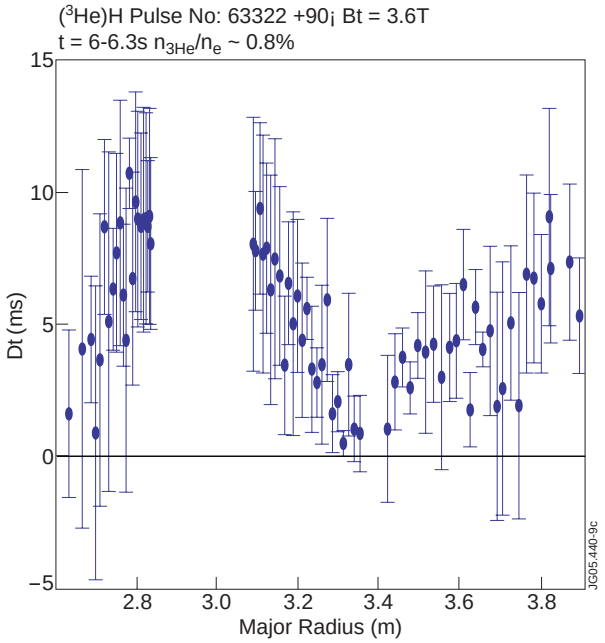

Figure 12: Time delay between the electron temperature response and the ICRF power modulation obtained with the new BIS method.

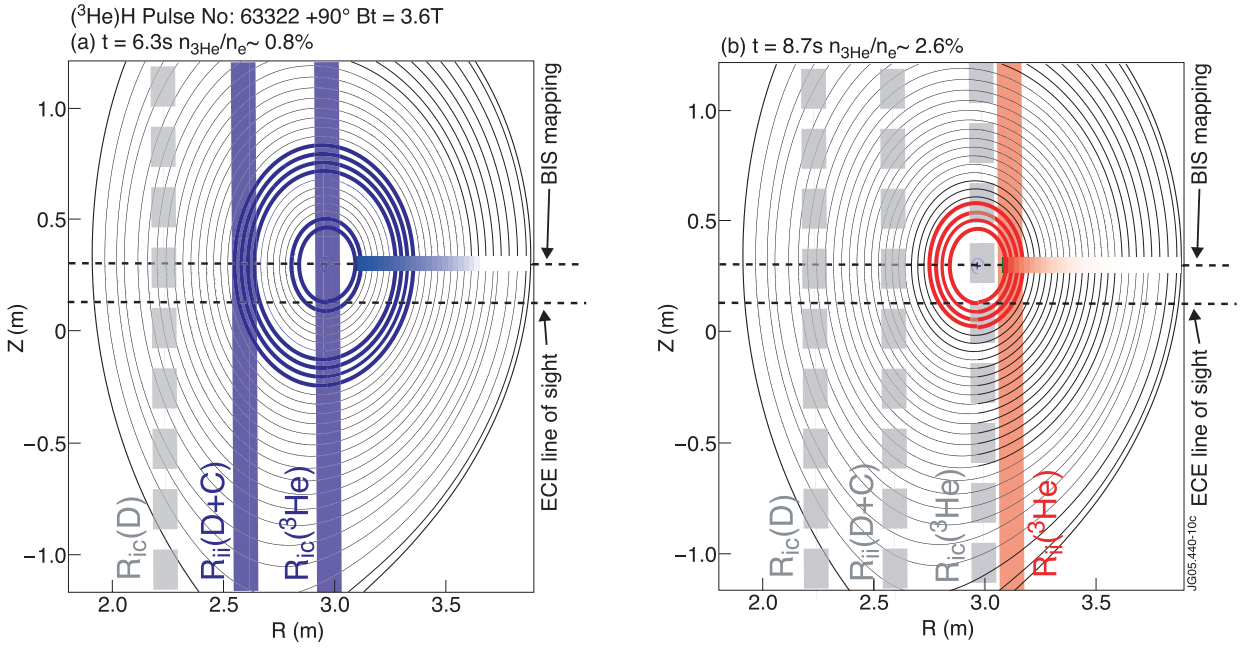

Figure 13: Tokamak poloidal cross-section with locations of the ^{3}He cyclotron resonance, D cyclotron resonance and associated ion-ion layers assuming 2% of D, 2% of C with B_t = 3.6T and an ICRF frequency of 37MHz. The line-of sight for the ECE electron temperature measurements and a cartoon of the BIS profiles are also shown. (a) is for $n_{3He}/n_e \approx 0.8\%$ and (b) is for $n_{3He}/n_e \approx 2.6\%$.

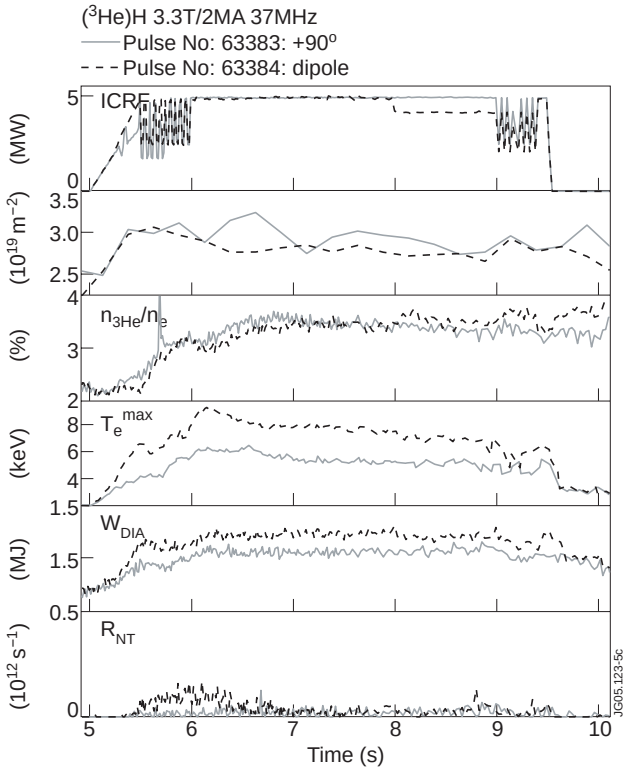

Figure 14: Time evolution of the ICRF power, central electron density from LIDAR Thomson scattering, ^{3}He concentration, maximum electron temperature from the ECE Michelson interferometer, plasma diamagnetic stored energy and neutron rate from ^{9}Be(^{3}He,n)^{11}C reaction. Two discharges are presented for dipole and +90° ICRF wave phasing.

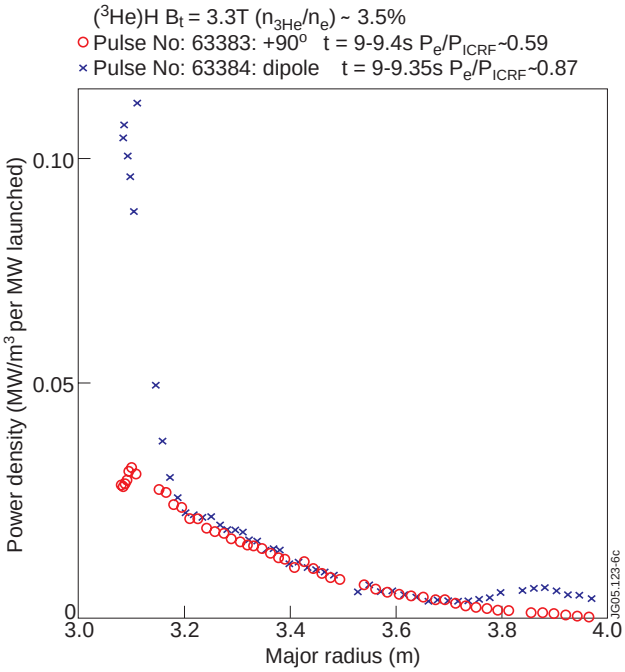

Figure 15: Direct electron deposition profiles from break-in-slope analysis for different pulses with similar ^{3}He concentration but different ICRF wave phasings.

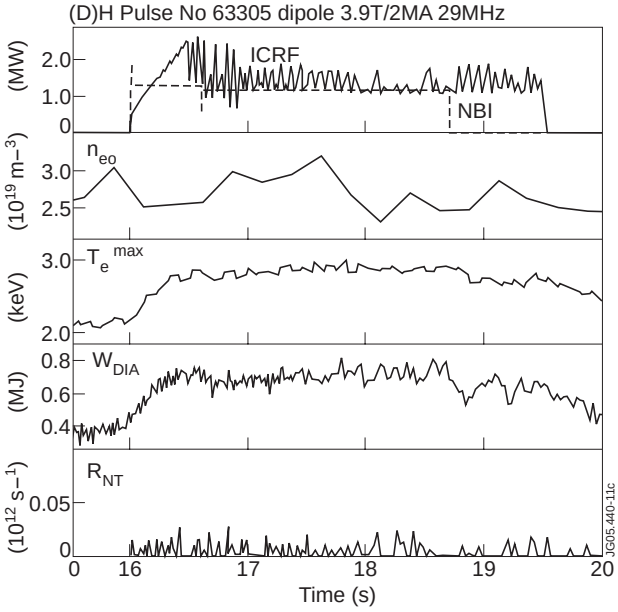

Figure 16: Time evolution of the ICRF power, NBI power (H beams), central electron density from LIDAR Thomson scattering, maximum electron temperature from the ECE Michelson interferometer, plasma diamagnetic stored energy and neutron rate.

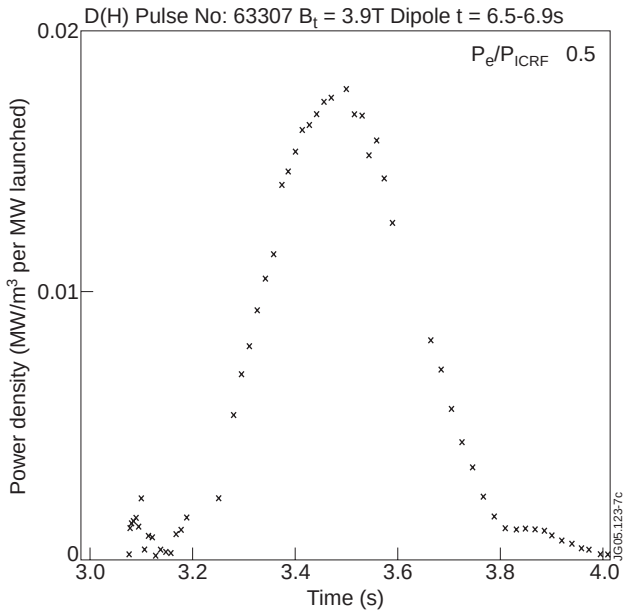

Figure 17: Typical direct electron deposition profiles from BIS analysis .

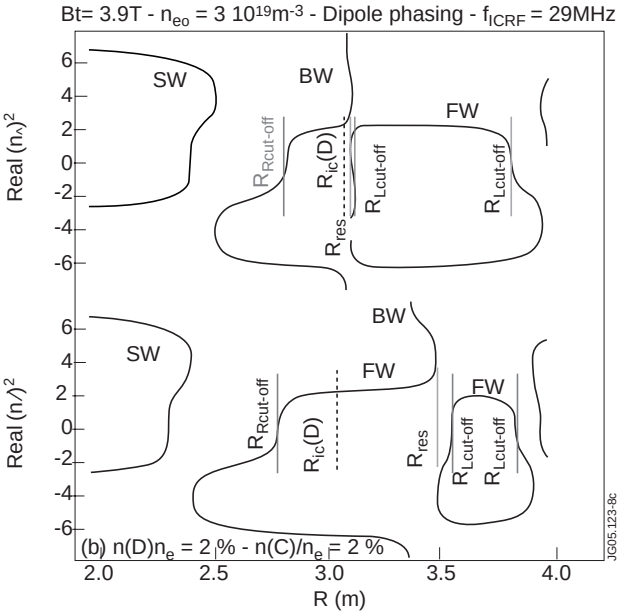

Figure 18: Real part of the perpendicular refractive index obtained from the resolution of the cold plasma dispersion relation. The following radial location are indicated: FW left cut-off $R_{Lcut-off}$*; FW right cut-off* $R_{Rcut-off}$*; FW resonance* R_{ii}*; D cyclotron resonance* R_{ic}*. Two cases are plotted: (a) with 2% of D and (b) with 2% of C and 2% of D.*

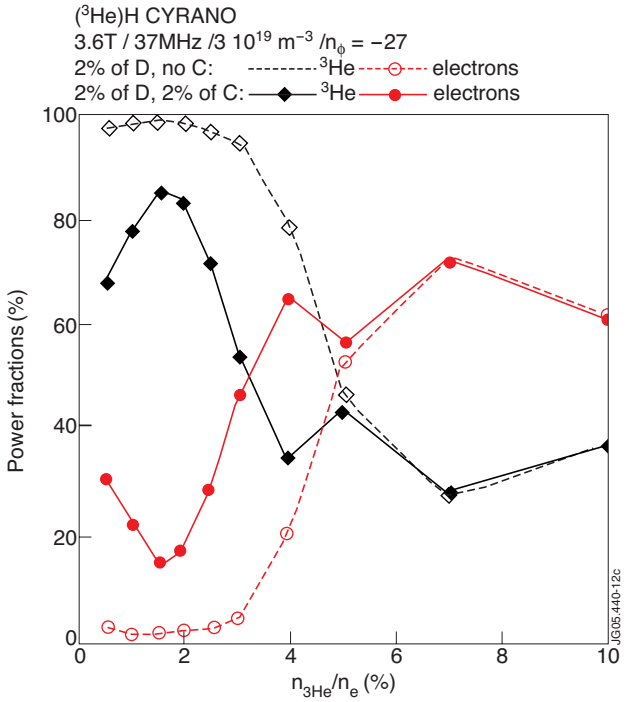

Figure 19: CYRANO simulations of the ICRF power going to the electrons and ^{3}He ions as a function of the ^{3}He concentration. Dashed lines are without carbon.

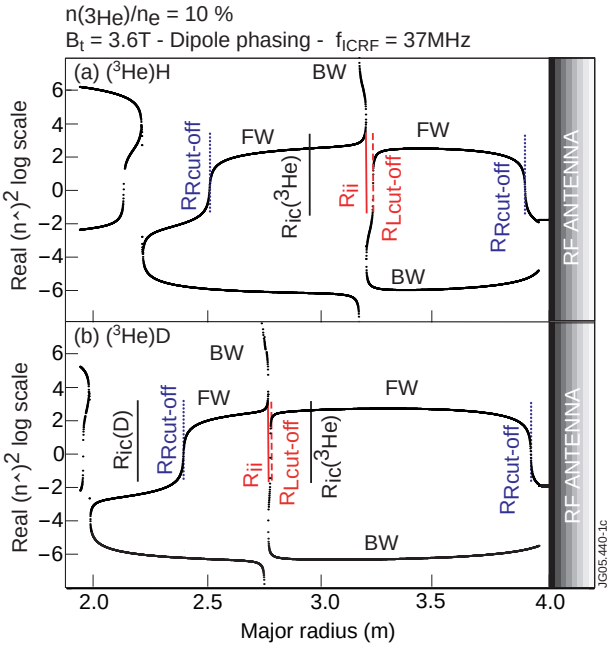

Figure 20: CYRANO simulations of power density profiles for a total input power of 1MW with 2% of D, 2% of C and ^{3}He concentration from 0.5 to 2%.

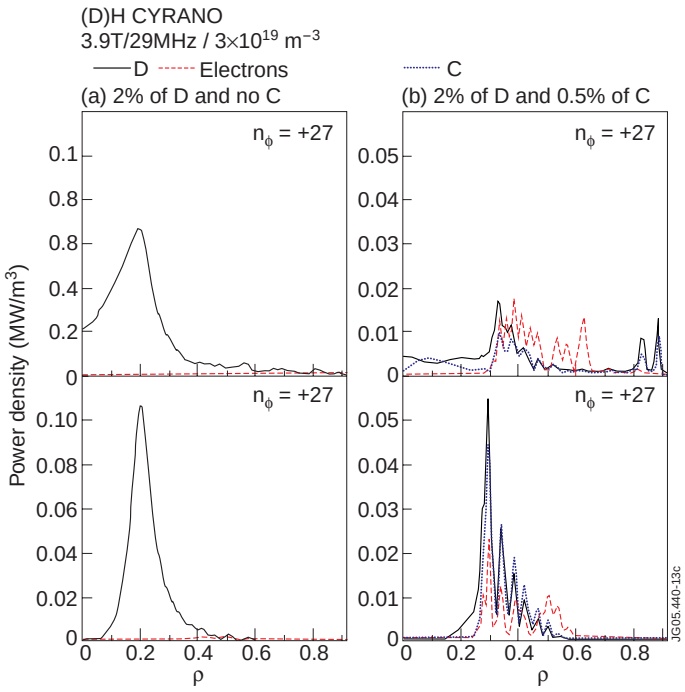

Figure 21: CYRANO simulations of power density profiles (a) without carbon and (b) with 0.5% of carbon. The total input power is 1MW and the toroidal mode numbers are $n_\phi = 27$ (bottom graphs) and $n_\phi = -27$ (top graphs).